An attempt to handle the nanopatterning of materials created under ion beam mixing

David Simeone, Gianguido Baldinozzi, Didier Gosset, Gilles Demange, Y. Zhang, Laurence Lunéville

Mater. Res. Soc. Symp. Proc. Vol. 1514 © 2013 Materials Research Society
DOI: 10.1557/opl.2013.449

An attempt to handle the nanopatterning of materials created under ion beam mixing

D. Simeone[1], G. Baldinozzi[2], D. Gosset[2], G. Demange[2], Y. Zhang[3], L. Luneville[4]
[1]DEN/DANS/DMN/SRMA/LA2M/LRC-CARMEN, CEA Saclay, 91191 Gif-sur-Yvette, France
[2]CNRS-SPMS/UMR 8580/ LRC CARMEN Ecole Centrale Paris, 92295 Châtenay- Malabry
[3]Materials Science & Technology Division, Oak Ridge National Laboratory, Oak Ridge, Tennessee 37831, USA
[4]DEN/DANS/DM2S/SERMA/LLPR/LRC-CARMEN, CEA Saclay, 91191 Gif-sur-Yvette, France

ABSTRACT

In the past fifty years, experimental works based on TEM or grazing incidence X ray diffraction have clearly shown that alloys and ceramics exhibit a nano pattering under irradiation [1,2,3]. Many works were devoted to study the nano patterning induced by ion beam mixing in solids [17,18,19]. Understanding the nano patterning will provide scientific bases to tailor materials with well-defined microstructures at the nanometric scale. The slowing down of impinging particles in solids leads to a complex distribution of subcascades. Each subcascade will give rise to an athermal diffusion of atoms in the medium. In this work, we focused on this point. Based on the well-known Cahn Hilliard Cook (CHC) equation, we analytically calculate the structure factor describing the nano patterning within the mean field approximation. It has shown that this analytical structure factor mimics the structure factor extracted from direct numerical simulations of the time dependent CHC equation. It appears that this structure factor exhibits a universal feature under irradiation.

INTRODUCTION

It is now well established that materials under irradiation exhibit unusual patterns [1,2,3,4]. Ion solid interaction is of significant interest to both academic and industrial researchers [1]. Ion implantation revolutionized the microelectronic industry offering a control over the number and depth of doping atoms in semiconductor materials [1]. Nowadays, the development of high current and high voltage implanters allows to tailor new compounds with new properties at the nanometric scale [5,6]. These unusual properties result from a steady state pattern formation induced by the slowing down of impinging particles under irradiation. From its ability to modify the local order over few nanometers, ion beam mixing appears to be a promising tool. However, elementary mechanisms responsible for this patterning are far to be clearly understood. Understanding the various mechanisms giving rise to both equilibrium and non equilibrium pattern formation in complex systems is a problem of long standing interest [7].

Two main reasons explain this lack of understanding. The slowing down of incident particles (ions, neutrons) leading to the creation of highly damaged area, termed thermal spikes or subcascades, is a stochastic process difficult to handle [8,9]. On the other hand, it remains difficult to handle the effect of a thermal spike on the microstructure of materials. From the seminal work of Martin and Bellon [10,11], it seems now well established that the effect of a thermal spike on the microstructure can be simulated by an athermal particle exchange. Such a

description can also be derived from the seminal work of Sigmund on the slowing down of particles in matter [12].

In this paper, we will focus on the second point and we will discuss the competition between two mechanisms: on one hand, an athermal displacement of atoms induced by a subcascade and on the other hand, the usual thermal driven mechanism trying to bring the solid to the thermo dynamical equilibrium. The steady state microstructure results from the balance between these two mechanisms. The first mechanism leads to destroy the long range order whereas the second tends to restore the long range order.

In the first part of the paper, we describe the effect of an athermal diffusion of atoms in a subcascade within the Landau framework of the Time Dependent Ginzburg Landau (TDGL) equation, extensively used to study the evolution of materials upon irradiation. The main interest of this work is to show critical parameters describing the subcascades able to generate a steady state nano patterning. Within this framework, we calculate the structure factor using a mean field approximation. In the second part of this work, we perform direct numerical simulations to compute this structure factor. The comparison between two structure factors allows assessing the different assumptions. In the last part of the text, we discuss the shape of the structure factor versus the irradiation parameters W and R.

MODELLING A SUBCASVADE WITHIN THE TDGL EQUATION FRAMEWORK

Even if at the microscopic level, the evolution of a material under irradiation can be described by an Ising model with a Glauber like spin flip kinetic, it remains possible to describe at a coarse grained level the microstructure of a material in terms of order parameters. Such a description was used to explain for instance the appearance of tetragonal zirconia nano crystals as well as the fragmentation of spinels under irradiation [2,4,12]. Such description also allows pointing out the amorphisation processes in glasses [13]. The TDGL was extensively used to describe the mechanism for phase separation in binary alloys. Cahn and Hilliard first introduced the conservative order parameter $\eta(r,t)=c_A(r,t)-c_B(r,t)$ to describe the spinodal decomposition of alloys. The evolution of the conservative order parameter $\eta(r,t)$ is given by Equation 1:

$$\frac{\partial \eta(\mathbf{r},t)}{\partial t} = M\nabla^2\left(\frac{\delta F}{\delta \eta}\right) \quad \text{(Eq.1)}$$

where M is the mobility derived from Onsager equation. In the following, we assume that M only depends on the average value of the concentration [21,22]. For an CuAg alloy, this mobility is independent of $\eta(\mathbf{r},t)$ and is equal to 487 s^{-1} out of irradiation at T=769 K. Moreover, only the free energy F depends on $\eta(\mathbf{r},t)$ and can be written as:

$$F(\eta(\mathbf{r},t)) = \int (f(\eta(\mathbf{r},t)) + \frac{\mu}{2}|\nabla \eta(\mathbf{r},t)|^2 dV \quad \text{(Eq.2)}$$

where f is the local coarse grained bulk free energy density. The term $|\nabla \eta(\mathbf{r},t)|^2$ has been added in the free energy to represent the energetic cost associated with interfaces. In order to describe

fronts, walls and labyrinthine patterns, the strength of the surface tension is given by the positive constant μ. We assume that f has a double well structure below a critical temperature T_c. All our analysis will be performed for temperatures below T_c. Under this assumption the simplest form of f is given by:

$$f(\eta(\mathbf{r},t)) = \frac{\alpha(T-Tc)}{2}\eta^2 + \frac{\beta}{4}\eta^4 \qquad \text{(Eq.3)}$$

The parameters α and β are positive constants. For a binary alloy, these coefficients can be identified by a comparison with the explicit form of the free energy F. For a CuAg alloy [23], the free energy of this alloy can be written as a regular solid solution out of irradiation. Its ordering energy and its unit cell parameter of the cubic structure are respectively equal to 0.0553 eV and 0.3 nanometer. For a temperature of 769K, coefficients α, β and μ are respectively equal to 1, 0.11 eV/nm^3 and 0.06 eV/nm^5. However, it is more appropriate to think of them as free parameters [2] without any reference to an underlying microscopic model.

The effect of thermal fluctuations can be incorporated in the Cahn Hilliard equation including a noise term θ(**r**,t). The resultant model is the well-known Cahn Hilliard Cook model [14]. As the noise at the equilibrium satisfies the fluctuation dissipation relation, we have $<\theta(r,t)> = 0$ and $<\theta(r,t)\ \theta(r',t')> = 2MkT\delta(r-r')\delta(t-t')$, where M is the mobility ($1.2\ 10^{-12}\ cm^2s^{-1}$ at T=769 K for CuAg out of irradiation). The bracket <.> denotes the average over the Gaussian noise ensemble. The presence of this noise insures that the system equilibrates to the correct Boltzmann distribution at equilibrium.

Such a model is also referred as the so called B model in the classification of Hohenberg and Halperin in the context of dynamical critical phenomena. The CHC model mimics the time evolution of A-rich and B-rich domains separated by interfaces. Before we proceed, it is relevant to discuss the applicability of the CHC model to real binary alloys at equilibrium. Lattice parameters mismatch in alloys and generate large strain fields. Such strain fields can be easily absorbed modifying the phenomenological coefficients of the bulk free energy density. This is one of success of this equation in material science as first pointed out by Katchaturyan.

Under irradiation, it is possible to add to the CHC equation an athermal diffusion of atoms due to a subcascade formation [11]. In a subcascade, atoms are set in motion during the thermal spike. During the thermal spike, complex defects like voids and dislocations are formed. However these defects do not evolve on the same time scale than the patterning does. These defects assumed to be shrunk are not taken into account to describe the evolution of the microstructure. On the other hand, point defects (vacancies and interstitials of the same species) move rapidly in the solid. It is well-known that these point defects enhance the atomic movement or diffusion at least in alloys and metals. We assume that these point defects only increase the value of the mobility M. For a subcascade of size L (about 10 nanometers), the thermal spike leads to a relocation of A and B atoms according to a simple diffusion equation [7,8]:

$$\frac{\partial \eta}{\partial t} = -W(\eta - p_R * \eta) \qquad \text{(Eq.4)}$$

where W describes the frequency of atom exchange and is a function of the atomic density of the material ρ (100 nm^{-3}), the mixing efficiency of the subcascade ς equal to 1 in the following and the flux of impinging particles ϕ (10^{-4} nm^2s^{-1}) [11]. The number of relocations occurring in a subcascade of size L reduces to ςρ/2 (5 10^4 atoms). The frequency associated with the occurrence of a subcascade at the same position in the solid reduces to ϕL^2 (10^{-2} s^{-1}). The "intensity" of the relocation W in a subcascade is then equal to 500 s^{-1}.

The function $p_R(r)$ is the probability for atoms belonging to the subcascade to be ejected at a distance *r* from its initial position. Molecular dynamic simulations [15] performed on alloys have shown that this function can be roughly mimicked with an exponential decay *exp(-r/R)*. R defines the spreading of this exchange occurring at the atomic scale (about 0.5 nanometers). The precise form of $p_R(r)$ seems not to play an important role to describe the patterns (see section II). When the parameters R or W tend to zero, the athermal driving term given by Eq.3 plays no role in the evolution of the microstructure. When R tends to infinity, the TDGL equation is similar to the usual equation describing the melting of a copolymer block and characterizes a chemical reversible equation mixing the two compounds [16]. Such an equation (R tends to infinity and W non null) is extensively used to discuss the phase separation in chemically reactive binary mixture. In this case, W is identified with the reaction constant of the reversible equation.

Combining the CHC equation with Eq. 4 leads to the TDLG equation allows studying the microstructure of binary alloys under irradiation. Whereas this equation is not based from first principles, this equation was applied to understand experimental results within a unified framework [2]. Such an equation can be considered as a toy model describing the patterning of materials observed under irradiation [17,18]. The characteristic value of W (500 s^{-1}) is of the same order of magnitude than the mobility M (487 nm^2 s^{-1}) for the CuAg alloy at 769 K. Under irradiation, a balance between the ordering of the alloy driven by the thermodynamic and the disordering induced by the athermal mixing inside the subcascade occurs. This balance may induce a patterning at the nanometric scale, i.e. the characteristic size of a subcascade, in this alloy.

The evolution of this alloy under irradiation is simply given by the TDGL equation. In this study, the initial configuration is given by the random high temperature microstructure quenched below T_c. To visualize this microstructure, The A-rich domains are marked black and B-rich domains are not marked. During the evolution of the alloys under irradiation, the average value of the order parameter $\frac{1}{V}\int \eta(\mathbf{r},t)dV$ is maintained null. Different parameter α, β, μ, M, W and R can be absorbed into the new definition of space and time by introducing rescaled variables for $T<T_c$ following a well-known procedure[19,20].

$$x' = x\sqrt{\frac{\alpha(T_c - T)}{\mu}}$$

$$t' = t\frac{M\alpha^2(T_c - T)^2}{\mu}$$

$$\eta' = \eta\frac{\beta}{\alpha(T_c - T)} \qquad \text{(Eq.5)}$$

$$W' = W\frac{\mu}{M\alpha^2(T_c - T)^2}$$

$$\theta' = \theta\frac{\sqrt{\beta\mu}}{M\alpha^2(T_c - T)^2}$$

θ' is a reduced noise with null mean value and a variance ε equal to $-2kT\Delta\frac{\alpha\sqrt{Tc - T}}{\sqrt{\mu}}$ -.

The micro structural evolution of the CuAg is then governed by the following equation:

$$\frac{\partial\eta}{\partial t} = \nabla^2(-\nabla^2\eta - \eta + \eta^3) - W(\eta - p_R * \eta) + \theta(r,t) \quad \text{(Eq.6)}$$

In this equation and in the following, the prime associated with reduced variables was dropped. The values of the order parameters and its second and quadric derivatives are null at the boundaries of the domain described by a subcascade exhibiting a cubic shape.

In previous attempts to catch the main feature of the patterns at low temperature created under irradiation, some authors [17] studied the stability of this equation at high temperature (T above T_c) where the conservative order parameter is null. This implies that the η^3 term is null. It appears then possible to apply the Bloch Floquet theorem to study the stability of different microstructures under irradiation [17]. However, such an analysis is unable to catch the features of the microstructure below T_c since the η^3 term is no more null and becomes the leading term in Eq. 6.

To overcome this difficulty, we use another approach to characterize the microstructure of systems under irradiation. This approach is based on a mean field approximation of the CHC equation [20]. The main interest of this approach is to determine the structure factor S(**k**,t) under irradiation. This function captures all the features of the microstructure. Within the mean field approximation, the effect of the noise on the microstructure has been neglected (ε=0). Following the formalism pointed out by previous authors [20], it is possible to calculate S(**k**,t) under irradiation for long times:

$$S(k,t)k_m(t)^3 = F(k/k_m(t), t\cdot g(WR^4)) \quad \text{(Eq.7)}$$

Eq. 5 clearly displays that the term $S(k,t)\ k_m(t)^3$ exhibits a Gaussian like shape and is a universal function of k/k_m and WR^4. Depending on the values of R and W, the wave vector $k_m(t)$ defining the patterning exhibits three distinct behaviors. The figure 1 summarizes these conditions:

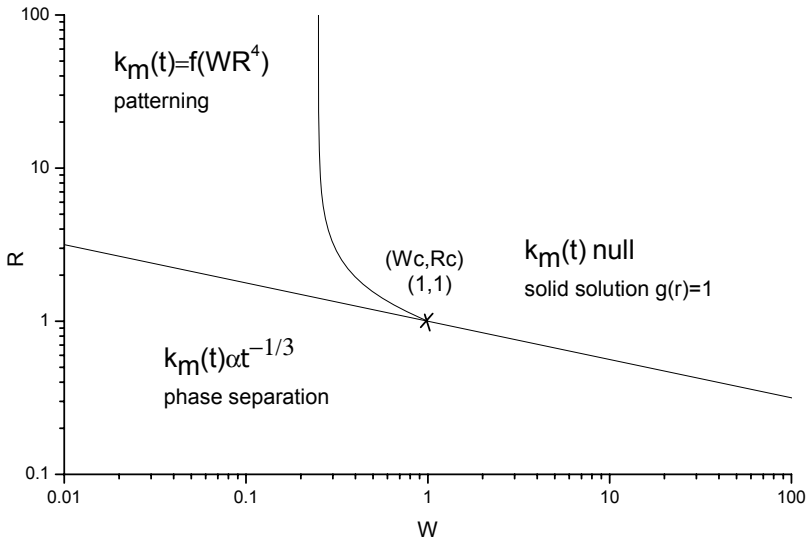

Figure 1: According to the reduced values of R and W, three distinct domains can be drawn. These domains are associated to a phase separation (low W values whatever R values are), a random solid solution (W is important and R above 1), and a steady state. This steady state is defined by a given value of k_m that only depends on W and R. As displayed on the graph, a critical point (Wc,Rc) equal to (1,1) appears.

From Eq. 7, it appears that the structure factor exhibits a Gaussian like shape peaked around a wave vector $k_m(t)$. Depending on different values of W and R displayed on figure 1, three distinct domains can occur under irradiation in a subcascade. For R and W values such that $WR^4<1$, the athermal motion of atoms occurring inside the volume of the subcascade is enable to avoid the demixion of the system. A phase separation occurs and the wave vector of the modulation $k_m(t)$ is a power law of t ($k_m(t) \sim t^{-1/3}$). Increasing the value of W, two distinct domains appear. For large R values ($WR^4>1$), $k_m(t)$ reaches a defined values function on W and R and independent of t. In this domain, a steady state is reached inducing a nano patterning inside the subcascade. For large W and R values, the athermal mixing of atoms resulting from chaotic collisions of atoms inside the subcascade disorder the alloy leading to the creation of a random solid solution. The boundaries layers of three domains intercept at a tri-critical point (Rc,Wc) as displayed on Figure 1. Boundaries of different domains calculated with our mean field approximation have an asymptotic expansion (R tends to infinity) in agreement to expressions obtained by previous authors studying chemical reactions [20]. The previous expressions of boundaries derived from the analysis of the stability [17] of Eq.4 do not satisfy these criteria. Even if the shape of the boundaries associated with three domains and the critical point are different than previous results [17], figure 1 exhibits qualitatively the same features than the one previously calculated [17]. The main interest of our work is to calculate the structure factor.

DIRECT NUMERICAL SIMULATIONS OF THE TDGL EQUATION

In order to assess the validity of the mean field approximation used to calculate S(k,t), we

directly compute the structure factor. Whereas the Kinetic Monte Carlo technique is extensively used to study the patterning induced by a subcascade [19], we solved Eq. 4 using a semi implicit finite difference scheme. Since the effect of a subcascade on the atomic concentration is a convolution product (Eq.3), we solve the equation in the Fourier space [25]. Applying an inverse Fourier transform to the Fourier components of the order parameter $\eta(\mathbf{r},t)$, it is possible to determine the patterns induced under irradiation in the real space.

We perform different simulations for different ε values (0.5, 0.01, 0.1, 0) and different R and W values. Results of simulations clearly showed that the thickness of the interfaces depends on ε. Larger ε is, broader the interfaces are. However, these results display that the long time characteristic size of domains does not evolve with ε. This result is in agreement with previous studies [24]. This point assesses the validity of the analysis within the mean field approximation framework. Figure 2 displays the evolution of the microstructure in the real space *for W=0.1* and *R=2*.

			
Fig 2a : (y,z) cut of the initial distribution of A and B atoms in a random AB alloy	Fig2b : evolution of the microstructure in the (y,z) cut for a reduced time of 100 ($\Delta y=\Delta z=0.4$)	Fig2c : evolution of the microstructure in the (y,z) cut for a reduced time of 500 ($\Delta y=\Delta z=0.4$)	Fig2d : evolution of the microstructure in the (y,z) cut for a reduced time of 1000 ($\Delta y=\Delta z=0.4$)

From the direct observation of the microstructure driven by irradiation, it appears clearly that a steady state is achieved (see figure 2c and 2d) for these values of W and R. In order to describe the microstructure more quantitatively, Figure 3 displays the evolution of the radial correlation function associated with these four patterns.

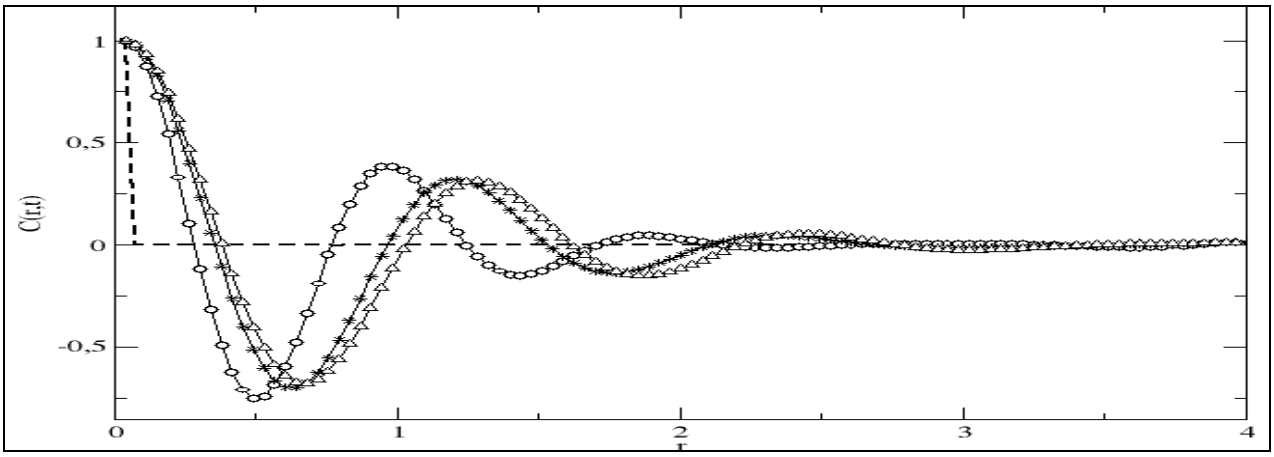

Figure 3. Evolution of the radial correlation function describing the evolution of η(x,y,z,t) in a subcascade under irradiation (W=0.1, R=2). At t=0, this function is a Dirac (dashed line) associated with the quenched random pattern. The radial correlation function exhibits a liquid like behavior (open dots). Increasing the time, oscillations associated with characteristic lengths appear around the reduced distance r=1and r=2 (open triangles and stars). For long times, this function no more evolves insuring the existence of a steady state for these values of R and W.

As the asymptotic expansion of boundaries displayed on Figure 1 are similar to those derived previously [20], it seems that the mean field approximation can be safely applied to capture the features of Eq. 4. However, to assess this point directly, the variation of k_m as a function of R is plotted on figure 4 for a given value of W for a long simulation time, when the steady state is achieved. To be sure the steady state is achieved; two distinct simulations using as initial configuration a random and a perfectly ordered state were performed. We check that the structure factors associated with two final states are similar; assessing the steady state is reached. Within our mean field approximation, it is possible to calculate $k_m(t)$ as a function of W and R. Figure 4 displays the evolution of $k_m(t)$ versus R for given values of W and t (black dots). As expected these points fall on the same line (full line) derived from the mean field approximation for WR^4 above 1. As predicted by our mean field approximation, this law vanishes for WR^4 below 1.

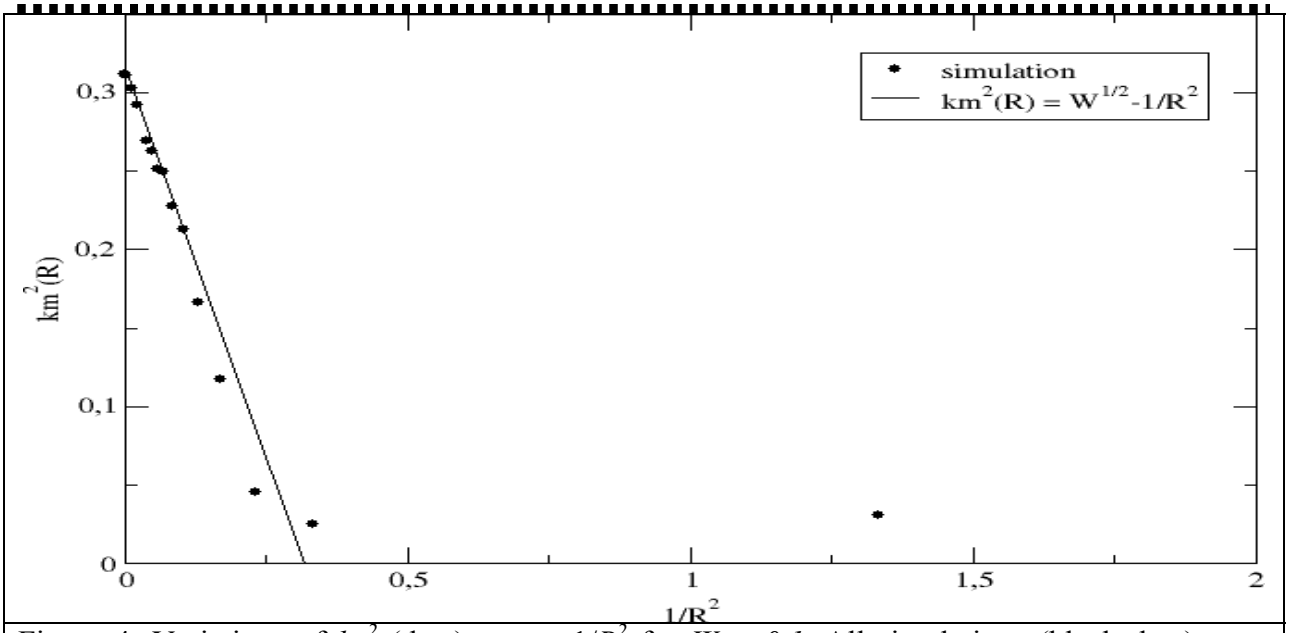

Figure 4: Variations of k_m^2 (dots) versus $1/R^2$ for $W = 0.1$. All simulations (black dots) were performed once the steady state is reached (the reduced time is kept to 2000 for all simulations). For WR^4 above 1, dots fall on the line derived from the mean field approximation. For WR^4 below 1, $k_m(t)$ do not evolve with R as expected by our approximation.

To assess the validity of the universal feature of $S(k,t)k_m^3$ in Eq.5, the structure factors associated with different values of W, R and t were calculated. Figure 5 displays the evolution of two structure factors $S(k,t)k_m^3$ as a function of k/km for a defined value of $tg(WR^4)$. Results extracted from simulations fall on the same universal Gaussian like curve (not plotted).

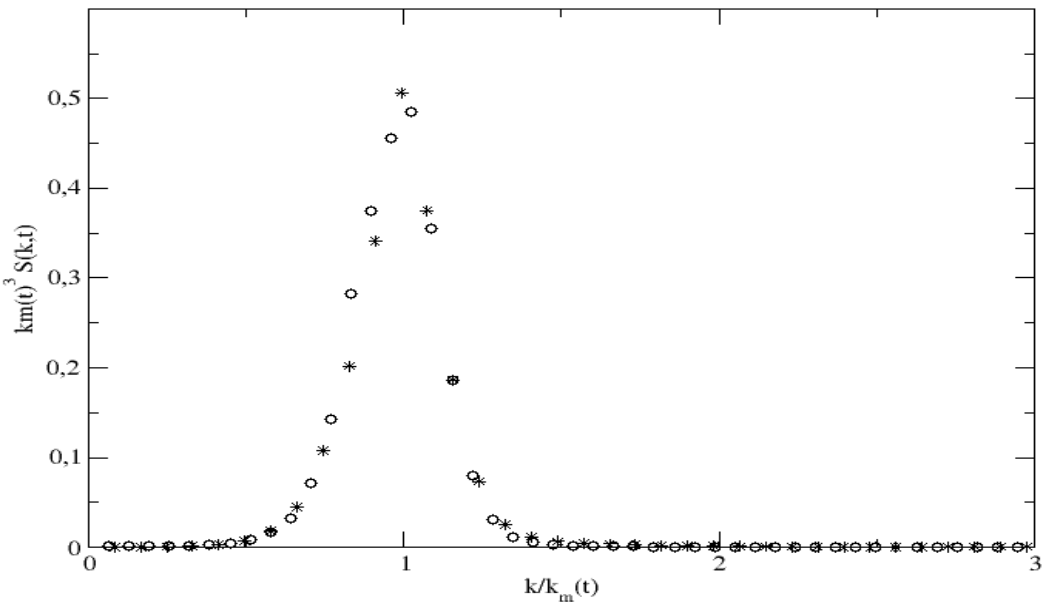

Figure 5: Plot of the normalized structure function as a function of k/k_m for different values of W, R and time extracted from numerical simulations. For a given value of $tg(WR^4)$, these two curves exhibit the same behavior as a function of k/k_m assessing the universal feature of $S(k,t)$.

The analysis of direct simulations of Eq.4 seems then to be accurately described within a mean field approximation framework as firstly pointed out by previous authors who have studied the structural evolution of diblocks copolymers out of irradiation [20].

DISCUSSION AND CONCLUSION

Since about fifty years, experimental works based on TEM or grazing incidence X ray diffraction have clearly shown that alloys and ceramics exhibit a nano pattering under irradiation [1,2,3]. Many works were devoted to study the nano patterning induced by ion beam mixing in solids [17,18,19]. Understanding the nano patterning will help to tailor materials with well-defined microstructures at the nanometric scale. The slowing down of impinging particles in solids leads to a complex distribution of subcascades. Moreover, each subcascade will give rise to an athermal diffusion of atoms inside the subcascade. In this work, we focused our attention on this last point. Based on the well-known Cahn Hilliard Cook equation, we analytically calculate the structure factor describing the nano patterning induced by irradiation inside a subcascade within the mean field approximation framework. We show that this analytical structure factor mimics the structure factor extracted from direct numerical simulations assessing the accuracy of our

approximation. From this analysis, it appears that this structure factor exhibits a universal feature under irradiation.

Since this work points out modifications of the microstructure of materials inside a subcascade, the following part of our work will be to study if and how different subcascades can modify this structure factor at a larger scale length. On the other hand, investigations are in progress to measure this structure factor from diffraction experiments.

REFERENCES

[1] Y. Cheng, Mater. Sci. Rep. **5**, 45 (1990).
[2] D. Simeone, G. Baldinozzi, D. Gosset, S. Le Caer, L. Mazerolles, Phys Rev B 70, 134116 (2004).
[3] A. Benyagoub, L. Levesque, F. Couvreur, C. Mougel, C. Dufour, E. Paummier, Appl. Phys. Lett. 77, 3197 (1998).
[4] G. Baldinozzi, D. Simeone, D. Gosset, I. Monnet, S. Le caer, L. Mazerolles, Phys Rev B 74, 132107 (2006).
[5] H. Bernas, J. P. Attane, K. H. Heinig, D. Halley, D. Ravelosona, A. Marty, P. Auric, C. Chappert, and Y. Samson, Phys. Rev. Lett. **91**, 077203 (2003).
[6] W. Bolse, Mater. Sci. Eng. R. **12**, 53 (1994).
[7] for a comprehensive review of spatio-temporal pattern formation in reaction diffusion systems, see M. Cross and P. Hohenberg, Rev Mod. Phys. 65, 851 (1993).
[8] D. Simeone, L. Luneville, Y. Serruys, Phys. Rev. E **82**, 011122 (2010).
[9] G. Martin, Phys. Rev. B 30, 1424 (1984).
[10] G. Martin, P. Bellon, Solid State Phys. **53-54**, 1 (1997).
[11] D. Simeone, L. Luneville, Phys. Rev. E 81, 21115, (2010).
[12] D. Simeone, C. Dodane, D. Gosset, P. Daniel, M. Beauvy, Journal of Nucl. Mat. 300, 151, (2002).
[13] H. Cook, Brownian motion in spinodal decomposition, Acta Metal. 18, 297, (1970).
[14] D Fisher, D. Huse, Phys. Rev. B 38, 373 , (1988).
[15] R Enrique, K. Nordlung, R . Averbach, P. Bellon, Journal of Applied physics 93(5), 2917, (2003).
[16]S. Glotzer, D. Stauffer, N Jan, Phys. Rev. Lett. 72,4109 (1994) .
[17] R. Enrique, P. Bellon, Phys. Rev. Lett. 84(13), 2885, (2000).
[18] R. Enrique, P. Bellon, Phys. Rev. B 63, 134111, (2001).
[19] J. Ye, P. Bellon, Phys. Rev. B 73, 224121 (2006).
[20] S. Glotzer, A. Coniglio, Phys. Rev. E 50(5), 4241 (1994).
[21] G. Martin , Phys. Rev. B 41, 2279, (1990).
[22] J.F. Gouyet, Phys. Rev. E, 51(3), 1695, (1995).
[23] L. Wei, R. Averback, J of Appl. Phys. 81, 613 (1997).
[24] T. Rogers, K. Eldere, R. Desai, Phys. Rev. B 37(16), 9638 (1988).
[25] J. Zhu, L. Cheng, J. Shen, V. Tikare, Phys. Rev. E 60(4), 3564, (1999).